ASTRONOMY & ASTROPHYSICS
SUPPLEMENT SERIES

Astron. Astrophys. Suppl. Ser. **136**, 385–394 (1999)

Atomic data from the IRON Project

XXXIV. Electron impact excitation of Fe XVI

W. Eissner[1], **M.E. Galavís**[2,4], **C. Mendoza**[3,4], **and C.J. Zeippen**[4]

[1] Lehrstuhl für Theoretische Physik I, Ruhr-Universität, D-44780 Bochum, Germany
[2] Departamento de Física, Universidad Metropolitana, PO Box 76819, Caracas 1070A, Venezuela
[3] Centro de Física, Instituto Venezolano de Investigaciones Científicas (IVIC), PO Box 21827, Caracas 1020A, Venezuela
[4] UMR 8631 (associée au CNRS et à l'Université Paris 7) et DAEC, Observatoire de Paris, F-92195 Meudon, France

Received September 25; accepted November 18, 1998

Abstract. As part of the IRON Project, electron impact excitation effective collision strengths are computed for the ion Fe XVI familiar in solar spectra. A Breit–Pauli R-matrix calculation is performed with a 12-level ($n \leq 4$) target representation. The calculation for this relatively simple ion is approached as a test case where we can analyze in detail most of the effects that contribute to the accuracy of the collision strengths: the energy mesh, relativistic corrections, the asymptotic multipole potentials and contributions from high partial waves. By comparing with two recent independent calculations, an accuracy rating of 10% is assigned to the present effective collision strengths in the electron-temperature range of $10^5 \leq T/K \leq 10^7$.

Key words: atomic and molecular data — sun: corona

1. Introduction

The international collaboration known as the IRON Project (IP, Hummer et al. 1993; Butler 1996) is concerned with a systematic treatment of the electron impact excitation of iron ions. A complete list of previous IP papers is available at `http://www.am.qub.ac.uk/projects/iron/papers/papers.html`.
In the present report we discuss the results for Fe XVI, an important ion in solar physics. Behring et al. (1976) identified some Fe XVI emission lines in the solar spectrum taken by a rocket-borne spectrograph in 1973. Sandlin et al. (1976) and Dere (1978) report on these lines with an accuracy of 0.03 Å. More recently, Thomas & Neupert (1994) have shown that all five transitions between the $n = 3$ configurations appear in the spectrum of an active region taken by the Solar EUV Rocket Telescope and Spectograph (SERTS) in its 1989 flight at $\lambda\lambda$ 251.067, 262.978, 265.018, 335.401 and 360.754 Å, measured with a precision of 5 mÅ. Young et al. (1998) have confirmed these identifications, and give some branching ratios and emission line ratios that are insensitive to density and temperature for these lines using the CHIANTI atomic data.

Emission-line ratios derived from transitions in Fe XVI can be used as diagnostics in high-temperature plasmas such as the corona, active regions and flares (Flower & Nussbaumer 1975; Vernazza & Reeves 1978; Dere 1978, 1982; Mason & Monsignori Fossi 1994; Dere et al. 1997; Brosius et al. 1997a). Keenan et al. (1994) have found good agreement between the observed and theoretical line ratios when they included the electron excitation rates computed by Tayal (1994) in their calculations. Furthermore, spatially resolved EUV emission-line profiles of this ion can be used to detect velocity fields in the low corona (Neupert et al. 1992); and simultaneous EUV and radio observations enable the coronal magnetic field structure to be interpreted (Brosius et al. 1993, 1997b). Fe XVI emission lines have also been observed in the EUV spectra of non-supergiant B stars (Cassinelli 1994), of the eclipsing binary Algol (Stern et al. 1995) and of the nearby K2 dwarf ϵ Eridani (Schmitt et al. 1996).

As a study object of atomic physics Na-like Fe XVI is a fairly simple ion. Hence we use this calculation as a test case to evaluate important effects that must be taken into account when studying electron impact excitation of highly ionized iron-group ions. The ultimate aim of the present work is to produce reliably evaluated collision data for astrophysical applications. With these goals in mind we compare the present results with the two most recent computations for this system: the 10 level close-coupling approximation by Tayal (1994), which takes into account

Send offprint requests to: C.J. Zeippen

the resonance structure at low energies, and a distorted wave calculation by Cornille et al. (1997). For reviews of earlier work see Badnell & Moores (1994) and Dere et al. (1997).

2. Method

In this work physical processes are described by the Hamiltonian

$$H^{\rm BP} = H^{\rm nr} + H^{\rm mass} + H^{\rm Dar} + H^{\rm so}, \quad (1)$$

where Breit–Pauli (BP) contributions of order $\alpha^2 Z^4\,{\rm Ry}$ are added to the non-relativistic Hamiltonian $H^{\rm nr}$; namely the mass–velocity, one-body Darwin and ordinary spin–orbit terms. The two-body components of relative BP-order $1/Z$ are neglected, which is adequate in our case. Each term of (1) involves N target electrons and a colliding electron, and $H^{\rm nr}$ includes a central potential due to an atomic nucleus with charge number Z. Thus expression (1) can be expanded in terms of states of total angular momentum and parity $J\pi$ when taking the entire Hamiltonian, and of states of total spin, orbital angular momentum and parity $SL\pi$ when the contribution $H^{\rm so}$ is neglected. We examine results obtained in either of these coupling schemes; they are connected by vector-coupling and term-coupling coefficients (TCC) and the transformation can be carried out at different stages of the calculation. This in turn affects computer time and accuracy.

2.1. R-matrix techniques

When collision-type trial functions (Burke & Seaton 1971) are used, the wavefunction for the total system of target and colliding electron is given by the expansion

$$\Psi^{J\pi} = \mathcal{A}\sum_i \chi_i \frac{F_i(r)}{r} + \sum_j c_j \Phi_j\ , \quad (2)$$

where $\mathcal{A}$ is the antisymmetrization operator, χ_i are vector coupled products of the target eigenfunctions and the angular part of the incident-electron functions, and the $F_i(r)$ are the radial parts of the latter. The functions Φ_j are bound-type functions of the total system introduced to compensate for orthogonality conditions imposed on the $F_i(r)$ and to render short-range correlations. The Kohn variational principle yields coupled integro-differential (ID) equations for the radial functions $F_i(r)$ for each angular symmetry.

R-matrix techniques (Burke et al. 1971; Berrington et al. 1974, 1978) are employed to solve the ID equations inside the R-matrix box (for $r \le a$, say).

2.2. Relativistic effects

One way to take relativistic effects into account is to employ the BP extensions which were first introduced in the R-matrix method by Scott & Burke (1980) and Scott & Taylor (1982). The target Hamiltonian is diagonalized in intermediate coupling. We make use of the resulting TCCs when recoupling the prior systems with respective $SL\pi$ symmetries to $J\pi$ symmetries, and we add the spin–orbit contribution from $H^{\rm so}$ due to the colliding electron.

To match to physical asymptotic boundary conditions a pair coupling scheme is adopted where the target angular momentum j is added to the orbital angular momentum l and spin s of the incident electron through an intermediate quantum number K (see, for example, Saraph 1972):

$$\boldsymbol{j} + \boldsymbol{l} = \boldsymbol{K} \quad \text{and} \quad \boldsymbol{K} + \boldsymbol{s} = \boldsymbol{J}\,. \quad (3)$$

Since spin–orbit coupling is negligible when $r \ge a$, no kinetic effects enter between the auxiliary states K and total angular momentum J. We make use of this fact when deriving expressions for contributions from high angular momenta.

The other recipe, computationally cheaper, is to first solve the coupled ID equations in the collisional $SL\pi$ symmetry. Then, following Saraph (1978), collision strengths between fine-structure levels are obtained by algebraic recoupling of the scattering matrices from LS to pair coupling. The method allows for term mixing via TCCs. So the relativistic effect of term mixing through spin–orbit interaction is obtained. However channel energies are degenerate for fine-structure levels associated with the same term. This approach will be referred to as the TCC method.

2.3. Long range potentials

The asymptotic region ($r \ge a$) is treated by the perturbative method described by Seaton (1985) and Berrington et al. (1987). In this region the ID equations reduce to the ordinary coupled differential equations

$$\left(\frac{{\rm d}^2}{{\rm d}r^2} - \frac{l_i(l_i+1)}{r^2} + \frac{2z}{r} + \epsilon_i\right) F_i(r) - \sum_{i'} V_{ii'}(r) F_{i'}(r) = 0\,, \quad (4)$$

where $z = Z - N$ is the residual charge of the ion, l_i and ϵ_i are the channel orbital angular momentum and energy of the colliding electron (in Rydberg units) and the quantities $V_{ii'}$ are long-range multipole potentials. Since asymptotically $|V_{ii'}(r)| \ll 2z/r$, these potentials can be treated by perturbation techniques. The asymptotic codes devised for the IP work allow for two options. Option 1: the potentials $V_{ii'}$ are included to first order, and Option 0: the potentials $V_{ii'}$ are neglected. Since computations with Option 0 are considerably less time consuming, we investigate its range of validity.

2.4. Contributions from high angular momenta

The high-l contribution to the collision strength (top-up) for optically allowed (oa) transitions is computed for

Table 1. Properties of the Fe XVI target orbitals: binding energy in the potential $V(\lambda_{nl})$, mean radius, last point of inflection (both after Schmidt orthogonalization) and cut-off radius of SUPERSTRUCTURE output

nl	λ_{nl}	ε_{nl}/Ryd	$\langle r/a_0\rangle$	$r_{\rm infl}/a_0$	$r_{\rm cut}/a_0$
1s	1.3910	−568.3753	0.0589	0.078	1.031
2s	1.0882	−95.8950	0.2649	0.344	0.781
2p	1.0283	−86.9523	0.2325	0.297	0.750
3s	1.0379	−35.5774	0.6811	0.891	0.750
3p	1.0060	−33.0837	0.6707	0.891	0.717
3d	1.0115	−29.6350	0.6134	0.828	0.719
4s	1.0000	−18.7545	1.2862	1.703	1.281
4p	1.0000	−17.8139	1.2903	1.703	1.434
4d	1.0000	−16.5456	1.2589	1.703	1.281
4f	1.0019	−16.0336	1.1197	1.484	1.031

Table 2. Comparison of experimental and theoretical energy levels (Rydberg units) for the Fe XVI target. Expt: Corliss & Sugar (1982). Pres: present results. T: Tayal (1994). CDMBB: Cornille et al. (1997)

i	Level	Expt	Pres	T	CDMBB
1	3s ^{2}S$_{1/2}$	0.000	0.000	0.000	0.000
2	3p ^{2}P$^{\rm o}_{1/2}$	2.526	2.519	2.552	2.530
3	3p ^{2}P$^{\rm o}_{3/2}$	2.717	2.701	2.741	2.716
4	3d ^{2}D$_{3/2}$	6.156	6.163	6.159	6.179
5	3d ^{2}D$_{5/2}$	6.182	6.193	6.208	6.209
6	4s ^{2}S$_{1/2}$	17.019	17.023	17.018	17.017
7	4p ^{2}P$^{\rm o}_{1/2}$	18.025	18.017	18.014	18.021
8	4p ^{2}P$^{\rm o}_{3/2}$	18.099	18.085	18.091	18.093
9	4d ^{2}D$_{3/2}$	19.357	19.355	19.370	19.364
10	4d ^{2}D$_{5/2}$	19.368	19.368	19.389	19.377
11	4f ^{2}F$^{\rm o}_{5/2}$	19.908	19.909		19.914
12	4f ^{2}F$^{\rm o}_{7/2}$	19.913	19.914		19.919

Table 3. Comparison of computed absorption oscillator strengths f_{ij} (length formulation) for the Fe XVI target. Pres: present results. T: Tayal (1994); CDMBB: Cornille et al. (1997); FMWY: Fuhr et al. (1981); SZF: Sampson et al. (1990). Hutton et al. (1988) give experimental values for the first two entries: 0.115 ± 0.007 and 0.244 ± 0.015

j	i	Pres	T	CDMBB	FMWY	SZF
2	1	0.125	0.127	0.147	0.125	0.124
3	1	0.269	0.272	0.269	0.272	0.269
4	2	0.294	0.291	0.294	0.294	0.291
4	3	0.028	0.028	0.028	0.028	0.028
5	3	0.255	0.253	0.255	0.254	0.251
6	2	0.058	0.059	0.062	0.062	0.060
6	3	0.063	0.064	0.067	0.066	0.064
7	1	0.072	0.071	0.076	0.076	0.079
7	4	0.033	0.033	0.034	0.034	0.034
7	6	0.184	0.185	0.181	0.182	
8	1	0.137	0.136	0.144	0.141	0.148
8	4	0.0063	0.063	0.642	0.0065	0.0064
8	5	0.039	0.039	0.039	0.039	0.039
8	6	0.393	0.394	0.389	0.393	
9	2	0.293	0.294	0.300	0.300	0.297
9	3	0.031	0.031	0.031	0.031	0.031
9	7	0.473	0.478	0.469	0.466	
9	8	0.045	0.045		0.044	
10	3	0.277	0.277	0.280	0.280	0.278
10	8	0.406	0.410	0.404	0.402	
11	4	0.921		0.923	0.924	0.892
11	5	0.044		0.044	0.044	0.043
11	9	0.114			0.111	
11	10	0.0053			0.0052	
12	5	0.880		0.881	0.882	0.853
12	10	0.107			0.104	

$J > J^{\rm oa}_{\rm max}$ with a procedure based on the Coulomb–Bethe approximation (Burgess 1974) and formulated by Burke & Seaton (1986) in the context of the R-matrix coding.

$$\sum_{l=\lambda+1}^{\infty} \Omega_{l,l-1} + \Omega_{l-1,l} = \left[\left(\frac{z^2}{\lambda^2}+\epsilon_2\right)\Omega_{\lambda,\lambda-1} - \left(\frac{z^2}{\lambda^2}+\epsilon_1\right)\Omega_{\lambda-1,\lambda}\right] \Big/ \left[\epsilon_1-\epsilon_2\right] \quad (5)$$

where $\Omega_{l,l'} = \Omega(i_1 l, i_2 l')$. The formulation requires just two partial collision strengths for each dipole allowed transition (i_1, i_2) at some $\lambda \approx L^{\max}$ (n.b. i stands for $\Gamma_i S_i L_i$ and $S_2 = S_1$ for these transitions). This procedure has been extended to intermediate coupling and details will be published elsewhere. For non-allowed (na) transitions we approximate the top-up for $J > J^{\rm na}_{\rm max}$ with a geometric series. Here $J^{\rm na}_{\rm max}$ is the highest J-value for which the ID equations are solved.

In order to assess the convergence of the partial wave expansion the resulting collision strengths are analyzed by means of the scaling techniques developed by Burgess & Tully (1992). The collision strength $\Omega(E)$ is mapped onto the reduced form $\Omega_{\rm r}(E_{\rm r})$, where the infinite energy range is scaled to the finite interval $(0, 1)$. For an allowed transition the scaled parameters $E_{\rm r}$ and $\Omega_{\rm r}$ are the dimensionless quantities

$$E_{\rm r} = 1 - \frac{\ln(c)}{\ln(\frac{E}{\Delta E}+c)} \quad (6)$$

$$\Omega_{\rm r}(E_{\rm r}) = \frac{\Omega(E)}{\ln(\frac{E}{\Delta E}+{\rm e})} \quad (7)$$

with ΔE being the transition energy, E the electron energy with respect to the reaction threshold and c is an adjustable scaling parameter. A key aspect of the approach by Burgess & Tully lies in the fact that the low as well as the high energy limits $\Omega_{\rm r}(0)$ and $\Omega_{\rm r}(1)$ are both finite and can be computed. For an electric dipole transition these limits are

$$\Omega_{\rm r}(0) = \Omega(0) \quad (8)$$

$$\Omega_{\rm r}(1) = \frac{4gf}{\Delta E} \quad (9)$$

where gf is the weighted oscillator strength (gf-value) for the transition. This method can also be extended to treat the effective collision strength

$$\Upsilon(T) = \int_0^\infty \Omega(E)\ \mathrm{e}^{-E/(\kappa T)}\mathrm{d}(E/\kappa T) \tag{10}$$

through the analogous relations

$$T_\mathrm{r} = 1 - \frac{\ln(c)}{\ln(\frac{\kappa T}{\Delta E} + c)} \tag{11}$$

$$\Upsilon_\mathrm{r}(T_\mathrm{r}) = \frac{\Upsilon(T)}{\ln(\frac{\kappa T}{\Delta E} + \mathrm{e})}\,, \tag{12}$$

where T is the electron temperature and κ the Boltzmann constant; the limits are

$$\Upsilon_\mathrm{r}(0) = \Omega(0) \tag{13}$$

$$\Upsilon_\mathrm{r}(1) = \Omega_\mathrm{r}(1)\ . \tag{14}$$

For a forbidden transition similar scaling relations are introduced by

$$E_\mathrm{r} = \frac{\frac{E}{\Delta E}}{\frac{E}{\Delta E} + c} \tag{15}$$

$$\Omega_\mathrm{r}(E_\mathrm{r}) = \Omega(E) \tag{16}$$

$$T_\mathrm{r} = \frac{\frac{\kappa T}{\Delta E}}{\frac{\kappa T}{\Delta E} + c} \tag{17}$$

$$\Upsilon_\mathrm{r}(T_\mathrm{r}) = \Upsilon(E) \tag{18}$$

with the following limits

$$\Omega_\mathrm{r}(0) = \Omega(0) \tag{19}$$

$$\Omega_\mathrm{r}(1) = \Omega_\mathrm{CB} \tag{20}$$

$$\Upsilon_\mathrm{r}(0) = \Omega(0) \tag{21}$$

$$\Upsilon_\mathrm{r}(1) = \Omega_\mathrm{CB} \tag{22}$$

where Ω_CB is the Coulomb–Born high-energy limit.

3. Target representation

The Fe XVI target is represented by a 12-level approximation: $3\mathrm{s}\,^2\mathrm{S}_{1/2}$, $3\mathrm{p}\,^2\mathrm{P}^\mathrm{o}_{1/2}$, $3\mathrm{p}\,^2\mathrm{P}^\mathrm{o}_{3/2}$, $3\mathrm{d}\,^2\mathrm{D}_{3/2}$, $3\mathrm{d}\,^2\mathrm{D}_{5/2}$, $4\mathrm{s}\,^2\mathrm{S}_{1/2}$, $4\mathrm{p}\,^2\mathrm{P}^\mathrm{o}_{1/2}$, $4\mathrm{p}\,^2\mathrm{P}^\mathrm{o}_{3/2}$, $4\mathrm{d}\,^2\mathrm{D}_{3/2}$, $4\mathrm{d}\,^2\mathrm{D}_{5/2}$, $4\mathrm{f}\,^2\mathrm{F}^\mathrm{o}_{5/2}$ and $4\mathrm{f}\ ^2\mathrm{F}^\mathrm{o}_{7/2}$. The wavefunctions are obtained with the structure code SUPERSTRUCTURE, originally developed by Eissner et al. (1974) and generalized by Nussbaumer & Storey (1978). A summary of the code's main features is given by Eissner (1991). In this approach the wavefunctions are expressed in a configuration expansion of the type

$$\Psi = \sum_i \phi_i c_i\ , \tag{23}$$

where the basis functions ϕ_i are constructed from one-electron orbitals computed in a Thomas–Fermi–Dirac–Amaldi statistical model potential $V(\lambda)$ as described by Eissner & Nussbaumer (1975) for $V(\lambda_l)$ and Nussbaumer & Storey (1978) for $V(\lambda_{nl})$. The scaling parameters λ_{nl} are computed variationally so as to minimize the weighted sum of the non-relativistic term energies. The λ_{nl} parameters for the present calculation are listed in Table 1 along with other properties of the target orbitals. Of particular relevance to the topping-up procedure are the last point of inflection and the mean radius of each orbital function. Tabulated radial functions are input to Stage 1 of the R-matrix code. Beyond the radial distance r_cut a Whittaker expansion can be employed up to the R-matrix radius of

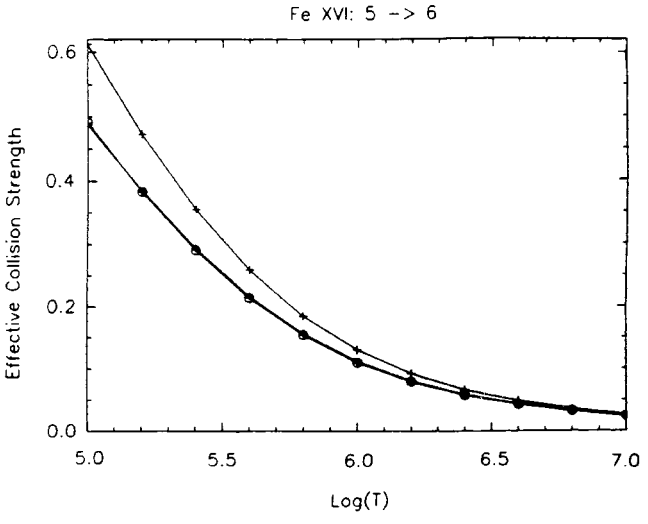

Fig. 1. Effective collision strength for the $3\mathrm{d}\,^2\mathrm{D}_{5/2} - 4\mathrm{s}\,^2\mathrm{S}_{1/2}$ transition in Fe XVI computed with different energy meshes. Crosses: $\delta E/z^2 = 5.0\ 10^{-5}$ Ryd. Asterisk: $\delta E/z^2 = 1.0\ 10^{-5}$ Ryd. Circles: $\delta E/z^2 = 5.0\ 10^{-6}$ Ryd. The residual charge of the system is $z = 15$. It may be seen that the latter two meshes lead to stable integration throughout the whole temperature region

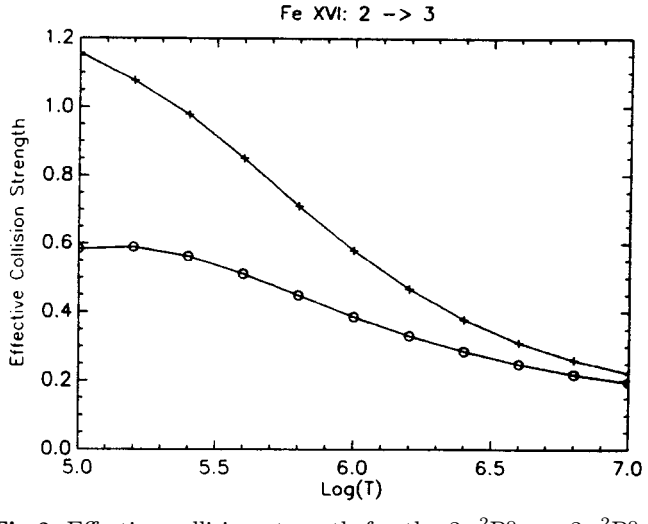

Fig. 2. Effective collision strength for the $3\mathrm{p}\,^2\mathrm{P}^\mathrm{o}_{1/2} - 3\mathrm{p}\,^2\mathrm{P}^\mathrm{o}_{3/2}$ transition in Fe XVI showing a large difference at low temperatures when the relativistic contributions are taken into account with the TCC method (crosses) and a Breit–Pauli calculation (circles)

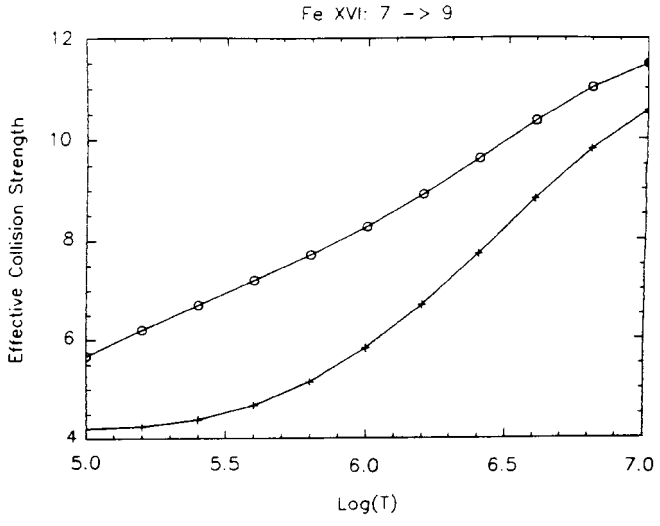

Fig. 3. Effective collision strength for the $4p\,^2P^o_{1/2} - 4d\,^2D_{3/2}$ transition in Fe XVI showing the large difference throughout the temperature range resulting from different treatments of the multipole potentials in the asymptotic region, see Sect. 4.3. Crosses: Option 0, Circles: Option 1

4.0 Bohr radii a_0; there the most diffuse orbital (4d) has decayed to relative magnitude 0.002.

For the present system it is relatively easy to obtain an accurate target representation. Internal consistency and comparison with previous calculations and experiment (see Tables 2 and 3) suggest an accuracy of the target level energies and f-values within the 2% uncertainty range. Note that levels 9 and 10 are labeled incorrectly in Table 2 of Tayal (1994), whereas they are tabulated correctly in the present Table 2. The reported computed oscillator strengths for the $4-8$ transition differ by up to a factor of 100. Varying the present λ_{nl} by as much as 10% would change our f-value of 0.0063 by not more than 20% (while unbalancing the excellent agreement between length and velocity results). Besides, the present oscillator strength for this transition agrees closely with the measurement listed in Fuhr et al. (1981) and the theoretical value obtained by Sampson et al. (1990). Other differences with the calculation by Cornille et al. (1997), namely for transitions $1-2$, $2-6$, $3-6$, $1-7$ and $1-8$ in Table 3, are small, and they can be explained as the result of alternative optimization procedures in SUPERSTRUCTURE such as different weighting in the variational functional or fewer variational parameters (perhaps λ_l rather than λ_{nl}).

4. Results

The resulting effective collision strengths for the electron-temperature range $10^5 \leq T/K \leq 10^7$ are listed in Table 6. We have used an R-matrix basis of 25 continuum orbitals, adequate for electron collision energies up to 200 Ryd. In the following sections each of the effects mentioned in Sect. 2 is discussed in detail.

Table 4. First point of inflection $r_{\rm infl}/a_0$ of selected partial waves associated with M-shell and N-shell channels for 2 energies measured from the ground state; the respective channel energies for $t > 1$ follow from Table 2 on averaging over fine structure, as t labels a term rather than a level i. Compare with $r_{\rm infl}$ from Table 1: $0.9\,a_0$ and $1.7\,a_0$

LS channel		100 Ryd			200 Ryd		
t	l	$L=15$	30	45	$L=15$	30	45
1	L	1.61	3.17	4.70	1.17	2.27	3.36
2	$L-1$	1.52	3.11	4.64	1.11	2.20	3.30
	$L+1$	1.73	3.30	4.86	1.27	2.36	3.45
3	L	1.64	3.27	4.83	1.17	2.30	3.39
	$L+2$	1.86	3.45	5.05	1.33	2.45	3.55
4	L	1.77	3.45	5.14	1.23	2.36	3.48
6	L	1.77	3.48	5.20	1.23	2.39	3.52
7	$L-3$	1.42	3.17	4.89	.984	2.14	3.30
	$L-1$	1.67	3.39	5.11	1.14	2.30	3.45
	$L+1$	1.89	3.61	5.33	1.30	2.45	3.61
	$L+3$	2.14	3.86	5.55	1.45	2.61	3.77

4.1. Energy mesh

The low-energy regime of the collision strengths for a highly ionized system such as Fe XVI is dominated by series of very narrow resonances. It would be computationally expensive to calculate such cross sections with an energy mesh fine enough to resolve all these features. However a practical choice must ensure stable integration when the rates are calculated. This is illustrated in Fig. 1, where the effective collision strength for the transition $3d\,^2D_{5/2} - 4s\,^2S_{1/2}$ has been plotted when computed with different mesh sizes. By comparing results obtained with steps of $\delta E/z^2 = 5.0\ 10^{-6}$ Ryd and $\delta E/z^2 = 1.0\ 10^{-5}$ Ryd ($z = 15$ is the residual charge of the ion), it is concluded that the latter mesh size is sufficiently fine while a mesh with a step of $\delta E/z^2 = 5.0\ 10^{-5}$ Ryd can lead to significant differences at the lower temperatures. Therefore cross sections are computed in the energy region below the highest threshold ($4f\ ^2F^o_{7/2}$) with a step of $\delta E/z^2 = 1.0\ 10^{-5}$ Ryd. In the region where all channels are open a wider step of $\delta E/z^2 = 1.0\ 10^{-3}$ Ryd is more than adequate.

4.2. Relativistic effects

As mentioned in Sect. 2, relativistic contributions are taken into account by either of two methods: by diagonalizing the Hamiltonian in intermediate coupling using a Breit–Pauli approximation, or, with less effort, by calculating reactance matrices in LS coupling before transforming to pair coupling using algebraic coefficients and TCCs. It is found that, for most transitions, effective collision strengths computed with the two methods are in

Table 5. $\Omega(3s\,^2S_{1/2}, 3p\,^2P^o_J)$ in intermediate and in LS coupling: Columns denoted 0^{17} and 1^{17} give results without and with multipole coupling respectively. The following 3 columns test the validity of the top-up formula when CC calculations go out to $J = 17$, 15 and 13 respectively. The lowest collision energy in the Table lies just above the highest target threshold

		OPTION$^{(J_{\max}\text{ or }L_{\max})}$					
ϵ_1	J	0^{17}	1^{17}	2^{17}	2^{15}	2^{13}	1^{13}
20	1/2	0.971	1.255	1.499	1.499	1.497	1.077
	3/2	1.954	2.454	2.902	2.892	2.878	2.080
	LS	2.925	3.711	4.424	4.422	4.419	3.165
50	1/2	0.874	1.032	1.805	1.803	1.800	0.813
	3/2	1.736	2.018	3.495	3.487	3.473	1.562
	LS	2.615	3.055	5.330	5.325	5.314	2.384
100	1/2	0.732	0.821	2.099	2.095	2.088	0.605
	3/2	1.450	1.601	4.082	4.072	4.054	1.157
	LS	2.187	2.429	6.208	6.194	6.156	1.773
200	1/2	0.548	0.588	2.391	2.371	2.315	0.386
	3/2	1.081	1.144	4.672	4.629	4.516	0.736
	Σ_J		1.737	7.063	7.000	6.831	1.122
	LS	1.635	1.738	7.063	6.962	6.709	1.130

good agreement. However for some transitions, particularly those arising within a term, the differences at low temperatures can be sizable as shown in Fig. 2. This is mainly caused by the neglect of the term energy splittings in the TCC method; i.e. energy-degenerate channels give rise to significantly different resonance patterns. Therefore it is advisable to adopt the full Breit–Pauli approach whenever possible.

4.3. Multipole-potential coupling

By comparing effective collision strengths computed with Options 0 and 1 in the asymptotic codes (see Sect. 2) it is possible to estimate the contributions from the long - range multipole potentials in the asymptotic region. Whereas for most forbidden transitions these contributions are small, it is found essential to include them in allowed transitions. For instance, it is shown in Fig. 3 that for the allowed transition $4p\,^2P^o_{1/2} - 4d\,^2D_{3/2}$ such differences can be fairly large throughout the temperature range of interest. A similar conclusion can be drawn when comparing the first two columns on the left in Table 5 which concerns the transitions $3s\,^2S_{1/2} - 3p\,^2P^o_J$. However it is found that when Option 1 is used numerical instabilities can crop up, particularly in the region just below a new threshold, causing the occasional abnormally high resonance. In the present work such features are eliminated by plotting the ratio of the two results with Options 1 and 0 in the resonance region and trimming any feature with a ratio larger than a factor of 5.

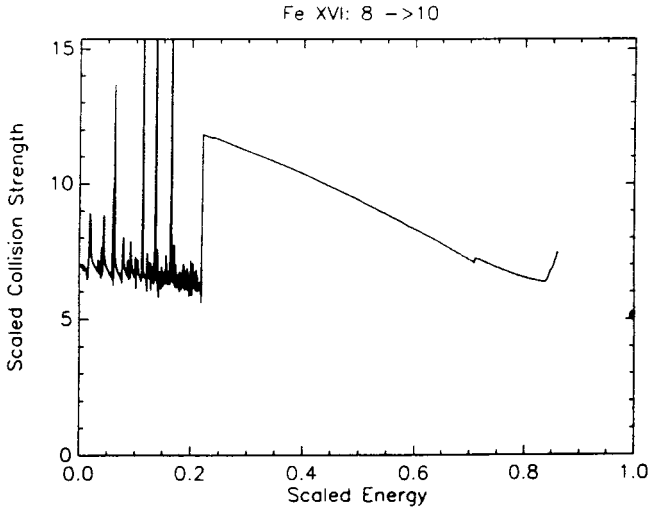

Fig. 4. Reduced collision strength plotted as a function of the scaled energy of Burgess & Tully (1992) (see Sect. 2) for the $4p\,^2P^o_{3/2} - 4d\,^2D_{5/2}$ optically allowed transition in Fe XVI showing the approach towards the high-energy limit (filled circle). It may be seen the breakdown that takes place at the higher energies due to an insufficiently high $J^{\rm oa}_{\max}$ (in this calculation $J^{\rm oa}_{\max} = 40$)

4.4. High-l top-up

Perhaps one of the most outstanding difficulties of the present calculation is the estimate of the contribution from the high partial waves. Collision strengths for optically allowed transitions must be topped up using the Burgess sum rules in some way. These rules can only be applied when the Bethe approximation without unitarization is valid. This means that the associated radial functions must have acquired their asymptotic forms. For bound orbitals this happens at some distance after their last point of inflection. For continuum orbitals one must go beyond their first point of inflection. Last points of inflection for the present target orbitals are listed in Table 1: $r_{\rm infl} = 0.9\,a_0$ for M-shell electrons, $1.7\,a_0$ for the N-shell. One can easily obtain an estimate of the first point of inflection of the continuum orbitals by solving the asymptotic form of the ID equations for high angular momenta and a range of energies. To an accuracy well within 10% one can say that

$$r_{\rm infl} \approx l/k \qquad \text{if} \quad E \gg z\,\text{Ryd} \quad \text{and} \quad l \gg 1\,. \tag{24}$$

These trends are illustrated in Table 4.

It is borne out by Table 5 that a ratio of *two* for the two competing radii gives acceptable results. Convergence is excellent once the first point of inflection of the partial waves appears at *three* times the radius of the last point of inflection of the respective target orbital. This condition is satisfied only at the first two energies for the M-shell transitions. For transitions involving electrons with principal quantum number $n = 4$ though this criterion is matched only at *much* higher values of angular momentum

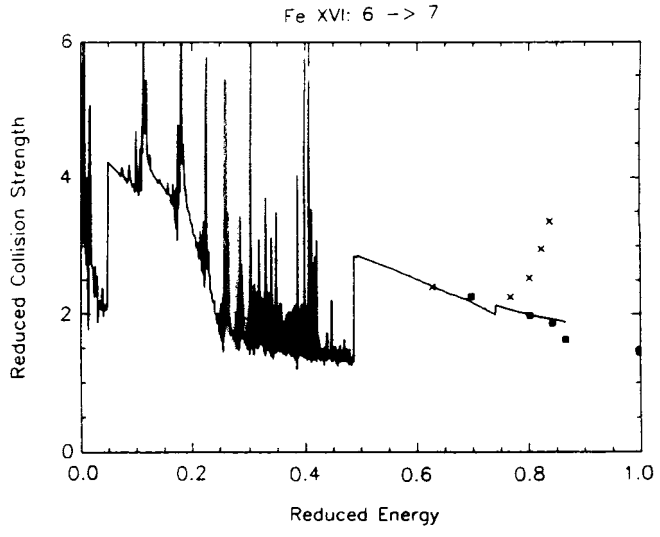

Fig. 5. Reduced collision strength for the $4s\ ^2S_{1/2} - 4p\ ^2P^o_{1/2}$ optically allowed transition in Fe XVI. Solid curve: present results. Crosses: Tayal (1994). Filled squares: Cornille et al. (1997). Filled circle: high-energy limit. The departure from the expected approach to the high-energy limit observed in the values by Tayal are believed to be due to an unreliable geometric series top-up

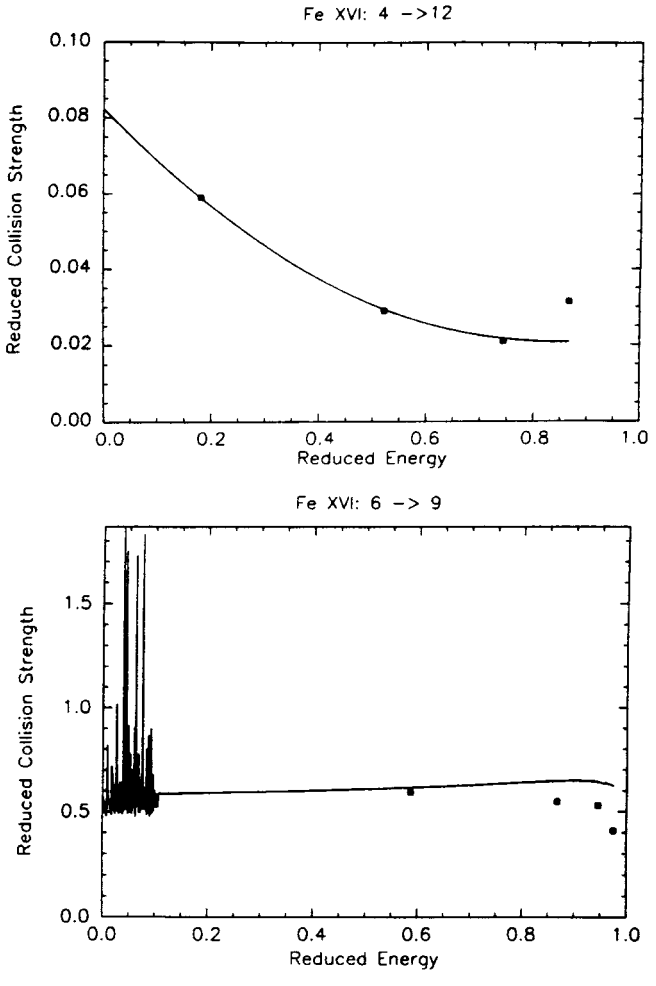

Fig. 6. Comparison of present collision strength (continuous curve) with those computed by Cornille et al. (1997) (filled squares). As shown for the transitions $4 - 12$ ($3d\ ^2D_{3/2} - 4f\ ^2F^o_{7/2}$) and $6 - 9$ ($4s\ ^2S_{1/2} - 4d\ ^2D_{3/2}$), the larger discrepancies are found for the high-energy point at 200 Ryd

l. In the present work we had to cut short the expansion with respect to angular momenta at $J^{\rm oa}_{\rm max} = 40$, fine at 100 Ryd but somewhat tight when approaching 200 Ryd (see Table 4). It suffices for most transitions in the region $E \leq 200$ Ryd, although for one or two of the more difficult cases incorrect high-energy tails required truncation at the breakdown point. This situation is illustrated in Fig. 4 with the allowed transition $4p\ ^2P^o_{3/2} - 4d\ ^2D_{5/2}$, where the collision strength is plotted using the scaling method of Burgess & Tully (1992). It may be seen that the reduced collision strength at high energies correctly approaches $\Omega_{\rm r}(1)$, but there is a point where this trend breaks down. This problem can certainly be alleviated by increasing $J^{\rm oa}_{\rm max}$ — at serious computational cost. The slow partial wave convergence in some quadrupole transitions is somewhat similar but not as acute; with a value of $J^{\rm na}_{\rm max} = 40$ and a geometric series top-up such transitions are accurately treated.

4.5. Comparison with previous work

The close-coupling calculation performed by Tayal (1994) for Fe XVI is very similar to the present. A striking difference lies in his treatment of the high partial waves, where for the optically allowed transitions a cut-off value of $J^{\rm oa}_{\rm max} = 15$ was adopted and a geometric series top-up was then implemented. For the forbidden transitions, on the other hand, Tayal considered the total collision strengths converged for $J^{\rm na}_{\rm max} = 15$. By contrast we find in the present work that reliable top-up procedures for some transitions, specially within $n = 4$ as discussed above, could only be safely introduced at much higher values of $J^{\rm oa}_{\rm max}$ and $J^{\rm na}_{\rm max}$, namely $J^{\rm oa}_{\rm max} = J^{\rm na}_{\rm max} \sim 40$. The convergence of some quadrupole transitions was found to be unusually slow. Tayal lists collision strengths at 5 energies in the non-resonant region (22.5, 36.0, 49.5, 67.5 and 90.0 Ryd) and effective collision strengths in the electron-temperature range $8\ 10^5 \leq T/K \leq 6\ 10^6$, thus facilitating a thorough comparison with present results. Cornille et al. (1997) have computed collision strengths for the fine-structure transitions with $n \leq 5$ at 4 energy points in the non-resonant region (26, 50, 100 and 200 Ryd). A distorted wave method with TCC recoupling is used for $L^{\rm oa}_{\rm max} = L^{\rm na}_{\rm max} = 19$ at 26 and 50 Ryd, and $L^{\rm oa}_{\rm max} = L^{\rm na}_{\rm max} = 24$ at 100 and 200 Ryd. For allowed transitions the Coulomb–Bethe top-up of Burgess & Shoerey (1974) is used in the range $L^{\rm oa}_{\rm max} < L \leq 200$. The 3s–$n$d quadrupole transitions are topped-up for $L > L^{\rm na}_{\rm max}$ with

Table 6. Present effective collision strength $\Upsilon_{ij}(T)$ for the electron impact excitation of Fe XVI

		log(T/K)										
i	j	5.0	5.2	5.4	5.6	5.8	6.0	6.2	6.4	6.6	6.8	7.0
1	2	1.31+0	1.29+0	1.28+0	1.27+0	1.27+0	1.28+0	1.31+0	1.38+0	1.48+0	1.61+0	1.76+0
1	3	2.41+0	2.43+0	2.44+0	2.46+0	2.48+0	2.51+0	2.57+0	2.70+0	2.90+0	3.15+0	3.43+0
1	4	1.34−1	1.37−1	1.42−1	1.47−1	1.51−1	1.52−1	1.51−1	1.47−1	1.45−1	1.44−1	1.43−1
1	5	1.99−1	2.05−1	2.14−1	2.22−1	2.28−1	2.30−1	2.27−1	2.23−1	2.18−1	2.15−1	2.14−1
1	6	1.38−1	1.27−1	1.18−1	1.10−1	1.04−1	1.00−1	9.84−2	9.80−2	9.85−2	9.96−2	1.01−1
1	7	2.69−2	2.33−2	1.96−2	1.63−2	1.38−2	1.22−2	1.17−2	1.22−2	1.38−2	1.67−2	2.07−2
1	8	4.58−2	4.11−2	3.53−2	2.97−2	2.55−2	2.28−2	2.19−2	2.29−2	2.60−2	3.14−2	3.90−2
1	9	2.58−2	2.32−2	2.11−2	1.96−2	1.87−2	1.84−2	1.87−2	1.94−2	2.07−2	2.24−2	2.43−2
1	10	3.80−2	3.41−2	3.10−2	2.90−2	2.78−2	2.74−2	2.78−2	2.90−2	3.09−2	3.34−2	3.64−2
1	11	3.65−2	3.66−2	3.66−2	3.66−2	3.66−2	3.67−2	3.68−2	3.70−2	3.72−2	3.76−2	3.79−2
1	12	4.87−2	4.88−2	4.88−2	4.88−2	4.89−2	4.89−2	4.91−2	4.93−2	4.97−2	5.01−2	5.06−2
2	3	5.81−1	5.84−1	5.60−1	5.11−1	4.52−1	3.93−1	3.41−1	2.96−1	2.61−1	2.34−1	2.17−1
2	4	1.70+0	1.71+0	1.73+0	1.76+0	1.79+0	1.84+0	1.91+0	2.01+0	2.15+0	2.33+0	2.53+0
2	5	5.72−2	6.25−2	7.29−2	8.41−2	9.18−2	9.26−2	8.34−2	7.34−2	6.27−2	5.41−2	4.70−2
2	6	1.04−1	8.53−2	6.69−2	5.11−2	3.91−2	3.07−2	2.57−2	2.35−2	2.36−2	2.59−2	3.00−2
2	7	1.38−1	1.33−1	1.26−1	1.21−1	1.16−1	1.13−1	1.12−1	1.12−1	1.12−1	1.13−1	1.14−1
2	8	4.37−2	3.94−2	3.40−2	2.86−2	2.42−2	2.10−2	1.88−2	1.77−2	1.73−2	1.75−2	1.81−2
2	9	6.86−2	6.14−2	5.59−2	5.27−2	5.17−2	5.31−2	5.72−2	6.48−2	7.65−2	9.31−2	1.14−1
2	10	2.79−2	2.47−2	2.19−2	1.97−2	1.81−2	1.67−2	1.56−2	1.47−2	1.39−2	1.33−2	1.28−2
2	11	1.07−1	1.08−1	1.10−1	1.12−1	1.15−1	1.19−1	1.26−1	1.34−1	1.44−1	1.55−1	1.68−1
2	12	2.60−2	2.57−2	2.53−2	2.46−2	2.37−2	2.26−2	2.13−2	1.99−2	1.86−2	1.75−2	1.67−2
3	4	4.19−1	4.27−1	4.43−1	4.63−1	4.80−1	4.87−1	4.96−1	5.01−1	5.18−1	5.43−1	5.77−1
3	5	3.17+0	3.20+0	3.24+0	3.31+0	3.37+0	3.45+0	3.56+0	3.75+0	4.00+0	4.32+0	4.70+0
3	6	2.28−1	1.86−1	1.45−1	1.11−1	8.45−2	6.66−2	5.59−2	5.13−2	5.19−2	5.72−2	6.63−2
3	7	5.55−2	4.76−2	3.95−2	3.25−2	2.70−2	2.31−2	2.06−2	1.92−2	1.88−2	1.90−2	1.98−2
3	8	3.34−1	3.19−1	3.00−1	2.82−1	2.68−1	2.58−1	2.53−1	2.51−1	2.52−1	2.55−1	2.58−1
3	9	4.64−2	4.17−2	3.78−2	3.48−2	3.29−2	3.17−2	3.14−2	3.20−2	3.37−2	3.66−2	4.06−2
3	10	1.52−1	1.37−1	1.25−1	1.17−1	1.14−1	1.16−1	1.23−1	1.37−1	1.59−1	1.90−1	2.30−1
3	11	6.53−2	6.52−2	6.50−2	6.48−2	6.45−2	6.43−2	6.44−2	6.49−2	6.62−2	6.83−2	7.09−2
3	12	2.07−1	2.09−1	2.11−1	2.14−1	2.19−1	2.26−1	2.35−1	2.49−1	2.65−1	2.85−1	3.07−1
4	5	2.64−1	2.78−1	3.29−1	4.01−1	4.54−1	4.63−1	4.16−1	3.55−1	2.88−1	2.32−1	1.85−1
4	6	3.42−1	2.68−1	2.02−1	1.48−1	1.06−1	7.59−2	5.47−2	4.06−2	3.16−2	2.59−2	2.26−2
4	7	2.63−1	2.25−1	1.81−1	1.40−1	1.05−1	8.04−2	6.41−2	5.48−2	5.12−2	5.22−2	5.67−2
4	8	1.59−1	1.40−1	1.16−1	9.07−2	6.97−2	5.35−2	4.19−2	3.38−2	2.86−2	2.55−2	2.41−2
4	9	4.53−1	4.04−1	3.64−1	3.35−1	3.14−1	3.00−1	2.91−1	2.86−1	2.84−1	2.83−1	2.84−1
4	10	1.04−1	8.63−2	7.22−2	6.11−2	5.24−2	4.53−2	3.93−2	3.40−2	2.96−2	2.59−2	2.30−2
4	11	9.17−1	9.26−1	9.40−1	9.61−1	9.93−1	1.04+0	1.11+0	1.20+0	1.34+0	1.51+0	1.71+0
4	12	7.91−2	7.75−2	7.52−2	7.19−2	6.76−2	6.21−2	5.58−2	4.92−2	4.28−2	3.71−2	3.23−2
5	6	5.45−1	4.25−1	3.21−1	2.35−1	1.69−1	1.20−1	8.62−2	6.38−2	4.93−2	4.03−2	3.50−2
5	7	1.63−1	1.33−1	1.03−1	7.74−2	5.72−2	4.22−2	3.14−2	2.38−2	1.85−2	1.48−2	1.23−2
5	8	4.89−1	4.29−1	3.49−1	2.71−1	2.07−1	1.59−1	1.27−1	1.08−1	1.00−1	1.00−1	1.06−1
5	9	9.11−2	7.80−2	6.68−2	5.76−2	5.02−2	4.39−2	3.84−2	3.35−2	2.93−2	2.58−2	2.30−2
5	10	7.11−1	6.35−1	5.73−1	5.27−1	4.95−1	4.73−1	4.58−1	4.49−1	4.43−1	4.41−1	4.41−1
5	11	1.51−1	1.50−1	1.48−1	1.46−1	1.44−1	1.41−1	1.40−1	1.39−1	1.42−1	1.48−1	1.58−1
5	12	1.35+0	1.36+0	1.38+0	1.41+0	1.45+0	1.52+0	1.61+0	1.75+0	1.93+0	2.16+0	2.42+0

the program NELMA (Cornille et al. 1994) based on a distorted wave approximation without exchange.

It is found that 85% of the collision strengths listed by Tayal (1994) agree with present results to within 10%. Large differences (up to 70%) are found, however, for optically allowed transitions with large collision strengths, in particular within the $n = 4$ terms (e.g. 4s−4p, 4p−4d). This situation is clearly illustrated in Fig. 5 with the 4s $^2S_{1/2}$ − 4p $^2P^o_{1/2}$ transition; it may be seen that the reduced collision strengths by Tayal show an increasing departure from the expected approach towards the high-energy limit. This finding seems to indicate that his geometric series top-up for allowed transitions can be unreliable at the high energies. On the other hand only 76% of the collision strengths by Cornille et al. (1997) are within the 10% level of agreement with the present data. Larger differences are mainly found towards the higher energies for the quadrupole transitions not arising from the ground

Table 6. continued

		log(T/K)										
i	j	5.0	5.2	5.4	5.6	5.8	6.0	6.2	6.4	6.6	6.8	7.0
6	7	3.25+0	3.22+0	3.39+0	3.69+0	4.07+0	4.50+0	4.98+0	5.50+0	6.08+0	6.70+0	7.33+0
6	8	6.76+0	6.62+0	6.87+0	7.40+0	8.08+0	8.86+0	9.75+0	1.07+1	1.18+1	1.30+1	1.43+1
6	9	5.85−1	5.88−1	5.92−1	5.97−1	6.02−1	6.09−1	6.17−1	6.25−1	6.31−1	6.34−1	6.36−1
6	10	8.81−1	8.83−1	8.86−1	8.92−1	9.00−1	9.10−1	9.22−1	9.33−1	9.43−1	9.49−1	9.51−1
6	11	1.09−1	1.09−1	1.08−1	1.07−1	1.05−1	1.04−1	1.03−1	1.02−1	1.01−1	1.01−1	1.02−1
6	12	1.45−1	1.44−1	1.43−1	1.42−1	1.40−1	1.38−1	1.36−1	1.35−1	1.35−1	1.35−1	1.36−1
7	8	1.51+0	1.35+0	1.20+0	1.08+0	9.86−1	9.16−1	8.62−1	8.21−1	7.88−1	7.60−1	7.37−1
7	9	5.56+0	6.16+0	6.72+0	7.24+0	7.75+0	8.31+0	8.97+0	9.73+0	1.06+1	1.16+1	1.27+1
7	10	1.97−1	1.82−1	1.70−1	1.61−1	1.54−1	1.50−1	1.47−1	1.46−1	1.46−1	1.47−1	1.48−1
7	11	5.84−1	5.87−1	5.90−1	5.95−1	6.00−1	6.05−1	6.11−1	6.17−1	6.21−1	6.23−1	6.23−1
7	12	7.61−2	7.49−2	7.32−2	7.09−2	6.80−2	6.47−2	6.13−2	5.80−2	5.52−2	5.29−2	5.12−2
8	9	1.34+0	1.46+0	1.56+0	1.66+0	1.76+0	1.87+0	2.00+0	2.16+0	2.33+0	2.52+0	2.70+0
8	10	1.02+1	1.13+1	1.23+1	1.33+1	1.42+1	1.53+1	1.65+1	1.78+1	1.94+1	2.11+1	2.27+1
8	11	2.66−1	2.65−1	2.64−1	2.62−1	2.60−1	2.57−1	2.54−1	2.51−1	2.48−1	2.45−1	2.43−1
8	12	1.06+0	1.06+0	1.07+0	1.07+0	1.08+0	1.08+0	1.09+0	1.10+0	1.10+0	1.10+0	1.10+0
9	10	7.32−1	6.70−1	6.16−1	5.71−1	5.33−1	5.01−1	4.73−1	4.49−1	4.28−1	4.10−1	3.96−1
9	11	1.13+1	1.15+1	1.17+1	1.19+1	1.23+1	1.30+1	1.40+1	1.53+1	1.67+1	1.81+1	1.95+1
9	12	1.52−1	1.48−1	1.43−1	1.36−1	1.28−1	1.19−1	1.09−1	1.01−1	9.34−2	8.79−2	8.42−2
10	11	9.82−1	9.89−1	9.97−1	1.01+0	1.03+0	1.07+0	1.13+0	1.21+0	1.31+0	1.40+0	1.49+0
10	12	1.61+1	1.63+1	1.66+1	1.69+1	1.75+1	1.83+1	1.94+1	2.09+1	2.25+1	2.41+1	2.56+1
11	12	5.60−1	5.44−1	5.22−1	4.93−1	4.59−1	4.19−1	3.78−1	3.38−1	3.03−1	2.73−1	2.49−1

state (i.e. 3d−4s and $n = n' = 4$) that have not been topped by Cornille et al. beyond $L^{\rm na}_{\rm max}$. In Fig. 6 we show two cases where discrepancies at $E = 200$ Ryd are greater than 30%; in the transition $3d\,^2D_{3/2} - 4f\,^2F^o_{7/2}$ it is seen that the agreement is excellent except for the value at 200 Ryd, which is 50% higher; for the $4s\,^2S_{1/2} - 4d\,^2D_{3/2}$ the situation is similar, but the high energy point is now 30% lower. The latter pattern is also found in the following transitions: $4s\,^2S_{1/2} - 4d\,^2D_{5/2}$; $4p\,^2P^o_{1/2} - 4p\,^2P^o_{3/2}$ and $4p\,^2P^o_{1/2} - 4f\,^2F^o_{5/2}$.

A comparison of the present effective collision strengths with those tabulated by Tayal (1994) in the electron-temperature range $8\ 10^5 \le T/K \le 6\ 10^6$ results in only 61% of the data agreeing to within 10% (82% to within 20%). In Fig. 7 we show two transitions with significant differences: $3s\,^2S_{1/2} - 4s\,^2S_{1/2}$ (up to a factor of two) and $3d\,^2D_{3/2} - 3d\,^2D_{5/2}$ (37%). Regarding the former, the high values at the lower temperatures listed by Tayal are due, in our opinion, to non-physical resonances caused by the numerical instabilities discussed in connection with the use of Option 1. The differences found in the transition within the $3d\,^2D$ term are more difficult to explain. Considerable differences are also found for $3d\,^2D_{5/2} - 4s\,^2S_{1/2}$ and for transitions with small (< 0.01) effective collision strengths.

5. Discussion

In the calculation of effective collision strengths for the Na-like ion Fe XVI we have examined in detail several effects that must be taken into account in order to ensure a reasonable level of accuracy. In particular the contribution of the high partial waves for both allowed and forbidden transitions has been found difficult to manage, as the top-up procedures can only be implemented at high values of the collisional J symmetry. In the present work we have adopted the values of $J^{\rm oa}_{\rm max} = J^{\rm na}_{\rm max} = 40$, which are adequate for most transitions although some of the allowed ones within the $n = 4$ complex still presented inacccurate high-energy tails that required truncation. We conclude from detailed comparisons with previous work that, in spite of the accuracy that is easily reached in target representation, the level of accuracy of the resulting effective collision strengths is probably not better than 10% for $\Upsilon > 0.1$ and 20% for the smaller ones. This is due to effects that come into play at high degrees of ionization. The present dataset is arguably the most reliable to date since we have made an attempt to identify the sources of error, and then take care of them so as to maintain accuracy. We have thus gained sufficient experience to tackle some of the more difficult iron ions that are being considered as part of the IRON Project.

Acknowledgements. Part of the present work was carried out during visits by MEG and CM to the Observatoire de Paris, Meudon, France. The hospitality received is gratefully acknowledged. The visits were funded by the CNRS, IVIC, CONICIT, Fundación Polar, the Observatoire de Paris and the Ministère des Affaires Étrangères. Computations were carried out at the Ohio Supercomputer Center, Columbus, Ohio, U.S.A., and at CeCalCULA, Universidad de Los Andes, Mérida, Venezuela. This research has been supported by CONICIT under contract No. S1-95000521. The authors are grateful to Dr. H.E. Saraph for a critical reading of the manuscript.

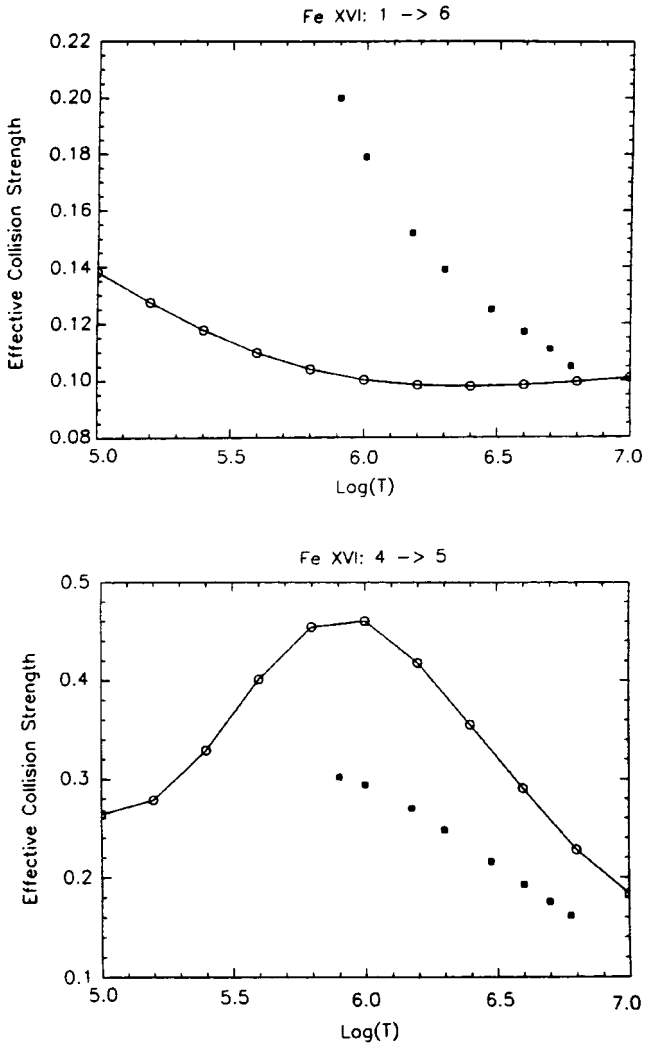

Fig. 7. Comparison of present effective collision strength (circles) with those computed by Tayal (1994) (filled squares). Although good agreement is found for most transitions, there are cases showing large discrepancies: for instance transition $1-6$ ($3s\,^2S_{1/2} - 4s\,^2S_{1/2}$) and transition $4-5$ ($3d\,^2D_{3/2} - 3d\,^2D_{5/2}$)

References

Badnell N.R., Moores D.L., 1994, At. Data Nucl. Data Tab. 57, 329
Behring W.E., Cohen L., Feldman U., Doschek G.A., 1976, ApJ 203, 521
Berrington K.A., Burke P.G., Butler K., et al., 1987, J. Phys. B 20, 6379
Berrington K.A., Burke P.G., Chang J.J., et al., 1974, Comput. Phys. Commun. 8, 149
Berrington K.A., Burke P.G., Le Dourneuf M., et al., 1978, Comput. Phys. Commun. 14, 367
Brosius J.W., Davila J.M., Thomas R.J., et al., 1997a, ApJ 477, 969
Brosius J.W., Davila J.M., Thomas R.J., et al., 1997b, ApJ 488, 488
Brosius J.W., Davila J.M., Thompson W.T., et al., 1993, ApJ 411, 410
Burgess A., 1974, J. Phys. B 7, L364
Burgess A., Shoerey V.B., 1974, J. Phys. B 7, 2403
Burgess A., Tully J.A., 1992, A&A 254, 436
Burke P.G., Hibbert A., Robb W.D., 1971, J. Phys. B 4, 153
Burke P.G., Seaton M.J., 1971, Meth. Comput. Phys. 10, 1
Burke V.M., Seaton M.J., 1986, J. Phys. B 19, L527
Butler K., 1996, Phys. Scr. T65, 63
Cassinelli J.P., 1994, Ap&SS 221, 277
Corliss C., Sugar J., 1982, J. Phys. Chem. Ref. Data 11, 135
Cornille M., Dubau J., Faucher P., et al., 1994, A&AS 105, 77
Cornille M., Dubau J., Mason H.E., et al., 1997, A&A 320, 333
Dere K.P., 1978, ApJ 221, 1062
Dere K.P., 1982, Sol. Phys. 77, 77
Dere K.P., Landi E., Mason H.E., et al., 1997, A&AS 125, 149
Eissner W., 1991, J. Phys. IV France 1, C1-3
Eissner W., Jones M., Nussbaumer H., 1974, Comput. Phys. Commun. 8, 270
Eissner W., Nussbaumer H., 1969, J. Phys. B 2, 1028
Flower D.R., Nussbaumer H., 1975, A&A 42, 265
Fuhr J.R., Martin G.A., Wiese W.L., Younger S.M., 1981, J. Phys. Chem. Ref. Data 10, 305
Hummer D.G., Berrington K.A., Eissner W., et al., 1993, A&A 279, 298
Hutton R., Engström L., Träbert E., 1988, Phys. Rev. Lett. 60, 2469
Keenan F.P., Conlon E.S., Foster V.J., et al., 1994, ApJ 432, 809
Mason H.E., Monsignori Fossi B.C., 1994, A&AR 6, 123
Neupert W.M., Brosius J.W., Thomas R.J., et al., 1992, ApJ 392, L95
Nussbaumer H., Storey P.J., 1978, A&A 64, 139
Sampson D.H., Zhang H.L., Fontes C.J., 1990, At. Data Nucl. Data Tab. 44, 209
Sandlin G.D., Brueckner G.E., Scherrer V.E., Tousey R., 1976, ApJL 205, L47
Saraph H.E., 1972, Comput. Phys. Commun. 3, 256
Saraph H.E., 1978, Comput. Phys. Commun. 15, 247
Scott N.S., Burke P.G., 1980, J. Phys. B 12, 4299
Scott N.S., Taylor K.T., 1982, Comput. Phys. Commun. 25, 349
Seaton M.J., 1985, J. Phys. B 18, 2111
Schmitt J.H.M.M., Drake J.J., Stern R.A., et al., 1996, ApJ 457, 882
Stern R.A., Lemen J.R., Schmitt J.H.M.M., et al., 1995, ApJ 444, L45
Tayal S.S., 1994, ApJ 426, 449
Thomas R.J., Neupert W.M., 1994, ApJS 91, 461
Vernazza J.E., Reeves E.M., 1978, ApJS 37, 485
Young P.R., Landi E., Thomas R.J., 1998, A&A 329, 291